SAND2016-7068C

Pressure Separation and Gas Flows in a Prototype Vacuum-Pumped Solar-Thermochemical Reactor

Ivan Ermanoski[1, a)], Adrian Orozco[1], and Johannes Grobbel[2]

[1]Sandia National Laboratories, PO Box 5800, MS 1415, Albuquerque, NM 87123, USA
[2]German Aerospace Center, Professor-Rehm-Straße 1, 52428 Jülich, Germany

[a)]Corresponding author: iermano@sandia.gov

Abstract. A detailed design of pressure separation by packed columns of particles, in a solar-thermochemical reactor prototype, is presented. Results show that the concept is sound and robust under a multitude of conditions anticipated in operation. Straightforward design features can be implemented to cover a wide range of contingencies.

INTRODUCTION

Two-step thermochemical cycles are a theoretically highly efficient and conceptually simple approach for solar fuel production. In the first step—thermal reduction—a reactive material (oxide) is partially or fully reduced at a high temperature. In the second step—fuel production—the reduced oxide is exposed to steam or CO_2 at a lower temperature, to produce H_2 or CO. Efficient two-step solar-thermochemical fuel production requires vacuum pumping or inert gas sweeping to lower the oxygen pressure in the thermal reduction step. Pumping is hampered by large oxygen volumetric flows, whereas sweeping is energy-intensive, requiring heat recovery at a high temperature, and a dedicated inert gas purification plant.[1-7]

A novel pumping approach— using a cascade of chambers at successively lower pressures—has been predicted to lead to over an order of magnitude pressure decrease compared to a single-chambered design.[8] To demonstrate the cascading reactor concept, as well as the whole cycle of a particle-based continuous H_2 production at realistic process temperatures and pressures, we have undertaken the design of a prototype device. This device includes two thermal reduction (TR) chambers, targeting ~100Pa and ~30Pa, while maintaining identical volumetric pumping speeds in both. The prototype is intended to be powered by a custom-built solar simulator, delivering a total of 3kW at the reactor apertures. The design is compatible with any oxide in particle form, though initially intended to operate with CeO_2.

The feasibility of pressure separation in a particle bed has been examined in some of our previous works, at a conceptual level.[9] However, an engineering solution for a reactor prototype demands a much more in-depth approach and rigorous analysis.

METHODS AND RESULTS

Design Requirements, Limitations, and Modeling Approach

Two main roles are served by pressure separation in the reactor prototype, shown in FIGURE 1. First, the flow of H_2 from the water splitting (WS) chamber to the O_2-containing thermal reduction (TR) chambers, must be small, to control recombination losses—i.e. loss of the desired H_2 product to recombination with O_2. Second, the flow of O_2 from the TR chambers (~1450°C) to the cooler segments of the reactor—especially the path between the TR2 and WS chambers—must also be small, to control recombination (reoxidation) losses between O_2 and the reduced oxide.

By design, these losses are intended to be so negligible that they can be omitted from efficiency considerations, such as those in [10, 11]. To fulfill these roles, the moving particle beds between reactor segments must not fluidize.

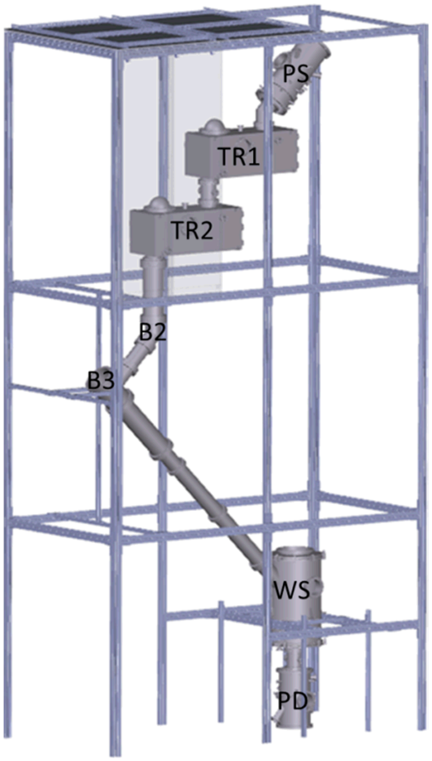

FIGURE 1. Cascading pressure reactor prototype schematic with two thermal reduction (TR) chambers and support structure. The reactor is ~7m tall. The reactive oxide is introduced to TR1 from the particle source (PS), then reduced in TR1 and TR2, at p_{TR1}=100Pa and p_{TR2}=30Pa, and T_{TR}~1450°C. The oxide is then exposed to steam, in the water splitting (WS) chamber to produce H_2, discharged into a particle drain chamber (PD), and finally returned (not shown) to PS to repeat the process. Separately pumped “buffer” chambers (B3 and B2) facilitate pressure separation between the ambient pressure in WS and TR2, maintained by the packed column of ceria particles between the two. The other design pressures in the reactor are: p_{WS}=83kPa, p_{B3}=10kPa, p_{B2}=800Pa. All except p_{WS} are to be maintained at the design level by controlling the corresponding vacuum pumping speed.

It is evident that best pressure separation results can be achieved by using narrow and long connecting tubes between the reactor chambers and fine reactive particles, which form low permeability packed beds. However, pressure separation requirements do not stand in isolation. The final design solution must also provide for reliable particle flow throughout the system, and a countercurrent steam-particle flow in the WS chamber, which therefore must not fluidize. These additional requirements suggest the use of wide connecting tubes (to prevent the formation of interlocking arches) and comparatively large particles (to prevent the formation of cohesive arches and to minimize the pressure drop along the WS chamber). Furthermore, vertical space limitations prevent the use of comfortably long (tall) pressure separation segments, so substantial design optimization is needed.

A column of particles standing off gas pressure must remain packed, must satisfy two main conditions. First, the “hydrostatic” pressure of particles above any vertical position in the bed (z), must be higher than the pressure difference between z and the top of the bed: $p_{bed}(z)>p(z)-p(z_{top})$. Put simply, the bed (column) as a whole must not be lifted by the gas pressure from below. Second, the gas exit velocity at the bed top must be lower than the particles' terminal (settling) velocity under the local conditions—i.e. individual particles must not be lifted by gas flow.

Understanding that the pressure is low in parts of the reactor, and viscous and molecular flow conditions may exist, care must be taken to apply the correct flow model. To determine the pressure as function vertical position in the bed, *p(z)*, we use the Ergun equation with a Knudsen correction factor, to account for different flow regimes:

$$\frac{\mathrm{d}p(z)}{\mathrm{d}z} = -\frac{\dot{m}_g}{A(z)}\frac{RT}{p(z)MD_p}\frac{1-\phi}{\phi^3}\left[\frac{150(1-\phi)\mu}{f_c\,(Kn)D_p} + 1.75\frac{\dot{m}_g}{A(z)}\right] \tag{1.}$$

Here, $\dot{m}_g$ is the gas mass flow through the bed, $A(z)$ is the bed cross-section area, M is the gas molar mass, D_p is the particle diameter, ϕ is the bed void fraction, μ is the gas dynamic viscosity, and T is the temperature. The Knudsen correction factor $f_c(Kn)$ depends on pressure and is calculated as follows:

$$f_c = [1 + \alpha(Kn)Kn]\left[1 + \frac{4Kn}{1-bKn}\right], \text{ where} \qquad Kn = \frac{\lambda}{D_p} \qquad \text{and} \qquad \lambda = \frac{k_B T}{\sqrt{2}\pi d^2 p} \qquad \text{(2)a, b, c.}$$

Here, Kn is the Knudsen number, λ is the gas mean free path, d is the gas molecules diameter (d_{H2}=0.297nm, d_{H2O}=0.275nm). The particle size is the characteristic dimension in which gas molecules move. The viscosities of hydrogen and steam are calculated based on the works of Stiel and Thodos, and Sengers and Kamgar-Parsi.[12, 13] The coefficient b=-1 is used for slip flow (i.e. one where Kn is large). The coefficient $\alpha(Kn)$ is calculated as follows:

$$\alpha(Kn) = \alpha_0 \frac{2}{\pi} tan^{-1}\left(\alpha_1 Kn^{\beta}\right), \qquad \text{where } \alpha_0 \equiv \alpha_{Kn\to\infty} = \frac{64}{3\pi\left(1-\frac{4}{b}\right)} \qquad \text{and} \qquad \beta = 0.4 \qquad \text{(3)2a, b, c.}$$

To apply Eq.(1), several assumptions were made. (1) the bed is considered stationary, (2) the net particle exchange between the gas and the solid is negligible, (3) bed temperature is uniform, (4) all particles have the same D_p, (4) the void fraction is uniform across the bed, and (5) that the problem can be treated 1-dimensionally.

Particle terminal velocity(v_t) is calculated from Stokes' law, with a Cunningham correction for slip flow:[14-18]

$$v_t = \frac{C(\rho_{solid} - \rho_{gas})D_p}{18} \qquad \text{where} \quad C = A \cdot Kn \qquad \text{and} \qquad C = \alpha + \beta e^{\frac{-\gamma}{Kn}} \qquad (4)$$

The coefficient A depends weakly on the specific gas and solid combinations[15, 19], so the same α, β, γ coefficients (for oil in air) were used for all gasses in our system (CeO_2 in H_2, O_2, and steam).

Results and Discussion

Pressure Separation Above the Water Splitting Chamber

We focus our analysis and results on the most challenging segment—pressure separation between the WS chamber and the TR chambers—with a large pressure difference (nearly 1atm) and ratio (~1000). The large difference necessitates a tall bed, and the large ratio requires gas expansion mitigation. Both are evident in FIGURE 1, manifested in the use of intermediate chambers B3 and B2, to gradually lower the pressure between the WS and TR chambers, and enable the pumping of permeating gasses at intermediate pressures. Both H_2 and steam are expected to be present in the gas flow from the WS chamber, and we examine them separately. To determine $p(z)$, and more generally $p(l)$ for a lengthwise position in non-vertical beds, Equation (1) is solved numerically.

Baseline case The pressure and superficial velocity (v_s) profiles for a baseline WS-B3 H_2 flow case are shown in FIGURE 2a. The assumed p_{WS}=82.8kPa is the ambient pressure in Albuquerqe, New Mexico. Also assumed are: particle diameter D_p=0.3mm, void fraction ϕ=0.4, bed height H=2.2m, (length L=3.1m inclined at 45°).

The superficial velocity is shown because in the ullage-like space at the bed top, it equals the actual gas flow velocity, relevant for the aerodynamic lift of individual particles. The flow is considered to be pure H_2—i.e. steam flow into the WS chamber is the minimal required, and a negligible steam amount is present following the reaction.

As is evident by the abrupt v_s drops, the diameter of the bed is not constant, but increases several times (starting at 15mm and ending at 100mm). Without diameter increases, no solutions exist, i.e. a mass flow value exists for which the final pressure is reached, but $p > p_{max}$ somewhere along the bed, indicating fluidization and a breakdown in the packed bed assumption. The diameter increases were chosen so that the pressure is comfortably below p_{max} in the entire bed (below 90% of p_{max}, in fact), not only to prevent fluidization, but also to ensure the existence of a net-downwards force to drive particle flow. As a contingency, should this force prove insufficient, the particle drain (PD in FIGURE 1) is a vacuum chamber, enabling sub-ambient pressure operation, down to a practical limit of ~10kPa, determined by reoxidation kinetics, and gas flow limits in the WS chamber.

The need for a staged pressure decrease (via B3 and B2), and the choice of p_{B3}=10kPa, are more evident in light of the need for bed diameter increases. Without pressure separation staging, the required bed expansion would quickly exceed practical diameters. Staging also allows the pumping of gasses flowing through the permeable bed "seal" with relative ease—at comparatively high pressures and low volumes.

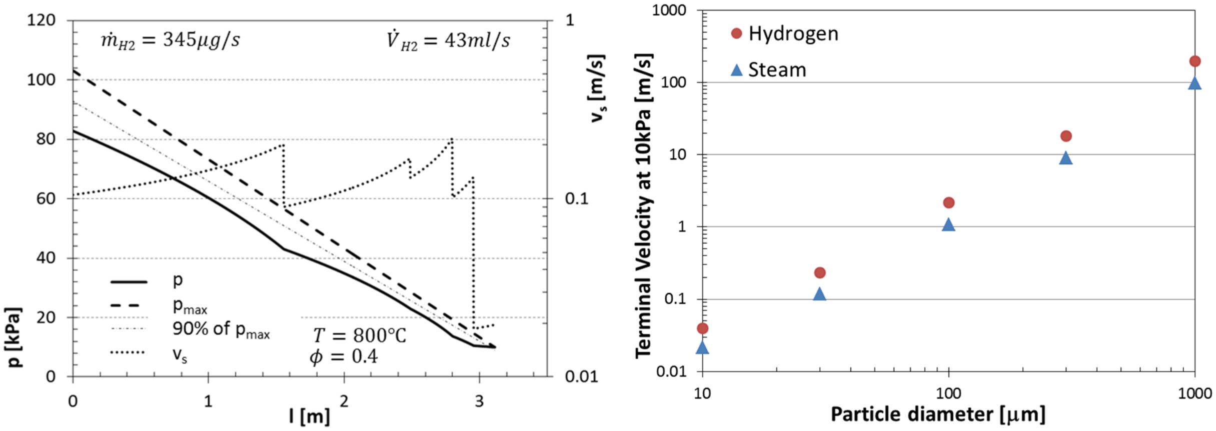

FIGURE 2. (a) Pressure and superficial velocity profiles for a baseline WS-B3 H_2 flow case. The solid black line is the pressure as function of length along the bed. The dashed line is the maximum "hydrostatic" pressure the bed above can sustain, based on its weight. The thin dash-dot line is 90% of that maximum pressure. The dotted line (right-hand axis) is the superficial velocity of the H_2 gas. (b) Terminal velocity of spherical ceria particles in hydrogen and steam, at 10kPa and 800°C.

The last bed diameter increase—at the top of the bed—serves to decrease v_s to a value that minimizes the lifting of fine particles, inevitably present in the system. Comparing v_s FIGURE 2b, we observe that particles of nominal size (D_p=0.3mm) have terminal velocities v_t far in excess of v_s at the top of the bed, and cannot be lifted. Only particles with D_p<20μm experience sufficient lift to be carried away from the top of the bed.

The mass ($\dot{m}_{H2}$) and volumetric (V_{H2}) H_2 flow rates across the bed, shown in FIGURE 2a, are miniscule. The volumetric flow rate is given at ambient temperature (27°C), to indicate the required pumping speed at B3, needed to maintain p_{B3}, and is well within the capacity of even small vacuum pumps. The volumetric flow at 800°C—i.e. at the top of the bed—is roughly 3.5 times higher (154ml/s). Finally, the flow rate at the pump outlet is lower by a factor of $p_{ambient}/p_{B3}$, and is approximately 5.2ml/s.

The calculated values for v_s show that the stationary bed approximation is valid. The expected ceria mass flow rate through the reactor is $\dot{m}_{CeO2}$≈2g/s. The solid density of ceria is ρ=7.2g/cm^3, giving a bulk density $\rho_{bulk}=\rho\phi$=4.32g/cm^3, yielding a flow velocity v_{CeO2}=2.6mm/s in the narrowest bed section—a value much smaller than the corresponding v_s≈150mm/s.

The oxide particles moving slowly through the reactor, it would be valid to ask if narrower beds would be a better design solution. Our experiments indicate that a 15mm diameter is near the limit of flow feasibility under the variety of conditions anticipated in the prototype, so its operation would be risked by using narrower beds. Nonetheless, in a larger and better characterized device, comparatively narrower beds (higher length to diameter ratios) would be feasible and probably advantageous.

Gas composition Before we explore the variety of possible conditions arising in operation, such as void fraction, temperature, particle size, etc., we examine the baseline case for steam flow in the WS-B3 segment, and show the results in FIGURE 3. This situation would approximately correspond to a steam feed rate into the WS chamber far in excess of the minimum needed for the oxide reoxidation.

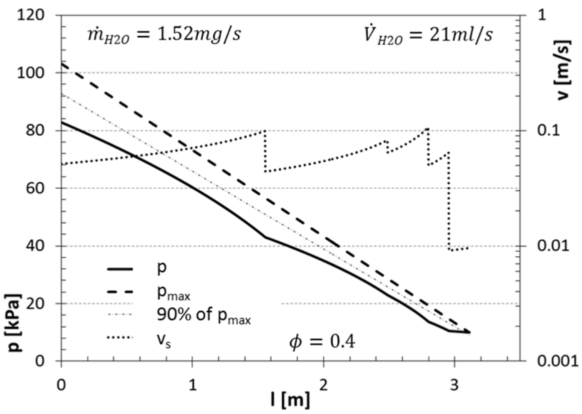

FIGURE 3. Pressure and superficial velocity profiles for a baseline WS-B3 H_2O (steam) flow case, with conditions identical to those in FIGURE 2a.

Some important observations can be made about these results. First, the pressure profile is identical to that in the case of H_2. This somewhat intuitive result, sets aside any concerns that fluidization could occur depending on a varying H_2/H_2O ratio in the WS chamber or along the bed. Second, the superficial velocity is roughly half of that for the H_2 case, and very much in line with the ratio of terminal velocities, thus allaying any concerns regarding particle lift at the top of the bed. Indeed, the only substantial difference—a higher mass flow, owing to the higher molecular mass of water compared to hydrogen—is of negligible experimental and operational consequence.

Effect of void fraction We now continue our analysis with an examination of the effects of operating parameters. While a void fraction of approximately 0.4 can be expected to be found in the prototype conditions, the steep dependence of Equation (1) warrants caution and further examination. To this end, we consider likely possible extremes of ϕ, corresponding to close random packing and loose random packing, and show the results in FIGURE 4.

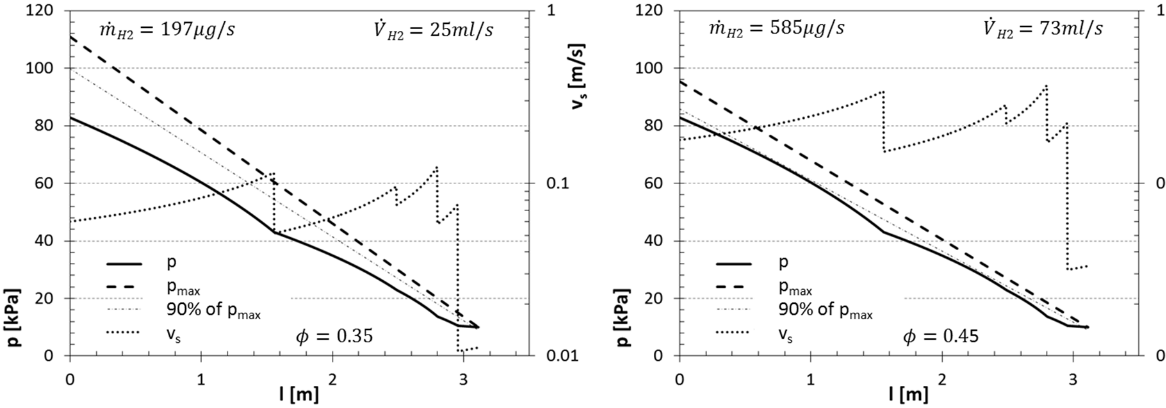

FIGURE 4. Pressure and superficial velocity profiles for void fractions below (ϕ=0.35) and above (ϕ=0.45) the baseline case in FIGURE 2a, with all other parameters equal.

The effects of varying void fractions are qualitatively intuitive: a lower void fraction (denser bed) gives a lower flow rate and higher margin between p and p_{max}, and vice versa. Importantly, the effects are relatively small, and do not bring into question the operation of the reactor, should the void fraction deviate from the baseline case, or even if variations are present along the bed. Considering the low required pumping speeds, it would appear that any void fraction scenario can be managed by adjusting the pumping speed at B3 and p_{WS}.

Effect of particle size It is rather unlikely that particles will be narrowly distributed around the design/baseline size D_p=300μm. In fact, one of the larger unknowns about the operation of a reactor of this type, is the equilibrium particle size distribution, achieved after long-term operation, and determined by the competing effects of attrition and sintering. To gain some understanding on the effects of particle size, we examine the baseline case for two additional sizes: D_p=100μm, and D_p=500μm (i.e. ±200μm from the baseline). The results are shown in FIGURE 5.

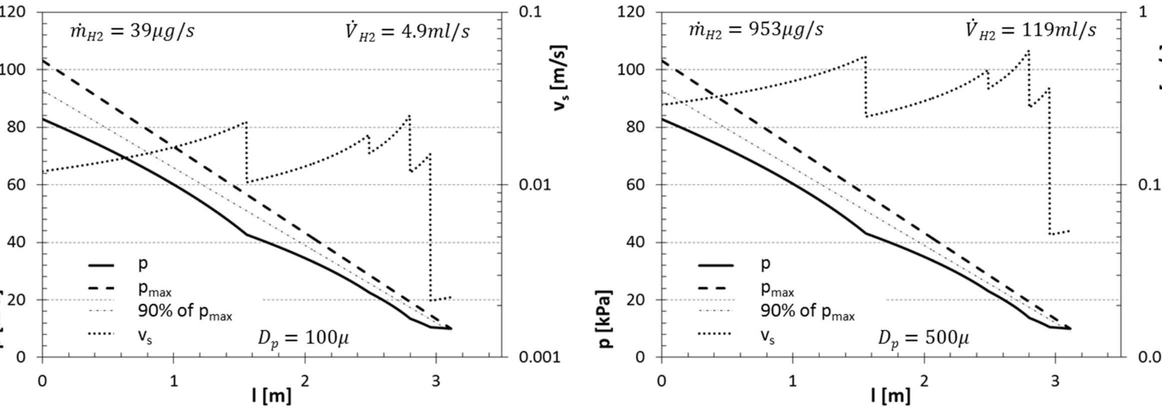

FIGURE 5. Pressure and superficial velocity profiles for particle a size below (D_p=100μm) and above (D_p=500μm) the baseline case in FIGURE 2a, with all other parameters equal. Note the different v_s scale between the plots.

Qualitatively, the results are in line with expectations: smaller particles lower the gas flow, owing to a smaller permeability. Quantitatively, it is very encouraging that the 100 μm particles so greatly diminish gas flow, yielding a roughly order of magnitude difference from the baseline 300 μm particles. On the other end, flow for 500μm particles is just under three times higher than the baseline. Much like previous cases, both situations can be managed by adjusting the B3 pumping speed and, if necessary, p_{WS}. The pressure profiles for both particle sizes are identical to the baseline, thus not jeopardizing the packed state of the bed.

With respect to gas flows, particle size within a relatively wide range of the baseline seems to be of little importance for reactor operation. Of much more concern would be any effects on particle flow, should the average diameter enter regimes of cohesive or interlocking arch formation. Without sufficient experience in operating a reactor, this must remain an open issue—one that can nonetheless be resolved by designing bed diameters appropriate for the equilibrium particle size.

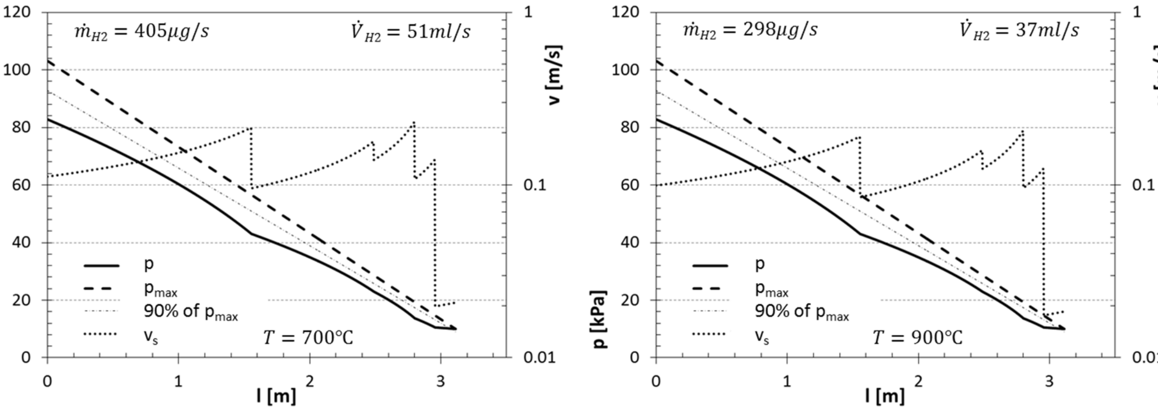

FIGURE 6. Pressure and superficial velocity profiles for temperatures below (T=700°C) and above (T=900°C) the baseline case in FIGURE 2a, with all other parameters equal.

The final factor we consider is temperature dependence, for two cases, one below (T=700°C) and one above (T=900°C) the baseline. Two somewhat competing effects play a role with temperature change. First, the viscosity of H_2 and steam (and gasses in general) increases with temperature, causing a decrease in mass flow. Second, gasses expand with temperature increase, causing an increase volumetric flow. The results are shown in FIGURE 6.

Evidently, temperature plays a minor role in pressure separation, with pressure profiles (again) identical to the baseline, and only minor differences in flow rates.

To briefly summarize the above results, they show that pressure separation by a slowly moving packed bed of particles is rather robust to the many conditions that may be encountered during operation, such as gas composition, void fraction, particle size distribution, and temperature. Variations in gas flows and pressure profiles arising from these conditions can be managed by modestly adjusting the pressure at the bottom of the bed and the pumping speed at its top.

The next bed section, B3-B2, with pB2=800Pa, bears some differences and some similarities with the WS-B3 section. The absolute pressure difference is smaller by a roughly order of magnitude, so the bed height needed to maintain pressure separation is also much smaller (designed at 35cm, compared to the 2.2m for WS-B3). The pressure ratio is somewhat higher, so bed expansion is still necessary, to the point that it drives bed height more than the pressure difference does. The latter is mitigated by a decrease in terminal velocity with decreasing pressure, allowing for higher superficial velocities at the top of the bed. A solution for this segment is shown in FIGURE 7, for a worst-case scenario (a high void fraction, and a lower than anticipated temperature).

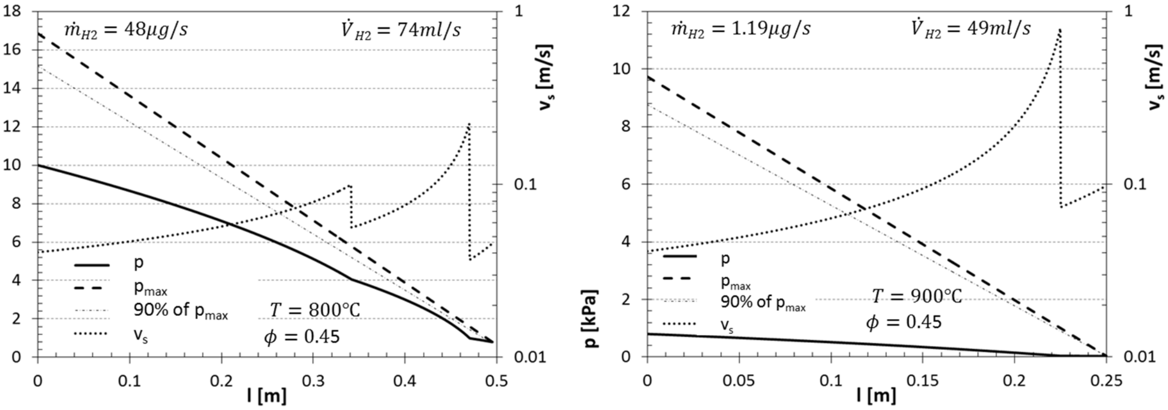

FIGURE 7. Pressure and superficial velocity profiles in the B3-B2 and the B2-TR2 sections (p_{B2}=800Pa, p_{TR2}=30Pa, ϕ=0.45).

Shown also in FIGURE 7 is the solution for the final segment, B2-TR2. Comparing $\dot{m}_{H2}$ between segments, it is evident that it decreases dramatically, with at most 1.2μg/s predicted to reach TR2, assuming all of the gas permeating through the particle column is H_2, and none is steam. This H_2 would recombine with the O_2 in the TR2 chamber. At the anticipated CeO_2 flow rate of 2g/s, the H_2 production rate is expected to be ~400μg/s, so the recombination rate would be at most 0.3%, i.e. of negligible magnitude in the prototype.

Pressure Separation Below the Thermal Reduction Chamber

An interesting problem arises in the segment(s) below thermal reduction chamber(s). The reduced oxide in these segments is no longer exposed to a (simulated) solar flux, which inevitably leads to some cooling. If the surrounding gas is similar in composition and pressure to that in the TR chambers, i.e. O_2 at p_{TR}, such cooling would lead to the swift reoxidation of the oxide, and a potentially significant loss of efficiency. To glean some understanding of the extent of the issue, we examine the potential losses for three idealized cases. We assume that reduced particles leave the TR2 chamber through a 15mm tube, and that they do not substantially cool in the first 100mm, 50mm, and 10mm of downward motion. For the design ceria mass flow rate $\dot{m}_{CeO2}$≈2g/s ($\dot{n}_{CeO2}$≈11.6mmol/s) and v_{CeO2}=2.6mm/s, this corresponds to 38s, 19s, and 3.8s of travel time. The O2 flow rate to a given depth in the bed depends on the pressure difference $\Delta p = p_{TR2} - p(z)$, so setting $p(z)$=0.1Pa, for example, is a satisfactory assumption, irrespective of the actual p_{O2} above the cooled reduced oxide. Using these assumptions, we calculate the O_2 mass flow rate $\dot{m}_{O2}$ to the three bed depths, and show the results in FIGURE 8.

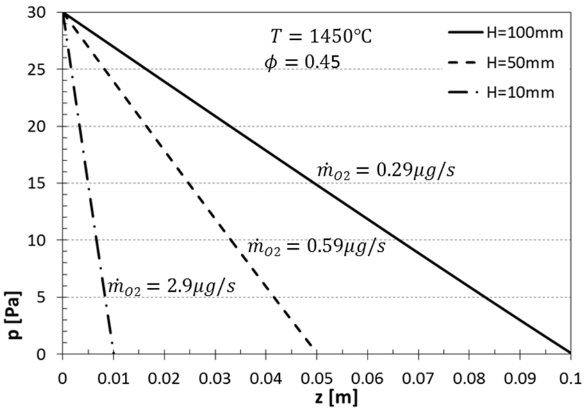

FIGURE 8. Oxygen pressure profiles between TR2 (p_{TR2}=30Pa) and three depths of a 15mm wide packed ceria bed at of 300μm particles 1450°C.

We compare the mass flow rates in FIGURE 8, with the design O_2 production rate in TR2. The extent of ceria reduction in TR2 (at 30Pa), is δ_{TR2}=0.01761, and in TR1 (at 100Pa), δ_{TR2}=0.01397, yielding $\Delta\delta$=0.00364 and $\dot{n}_{O2,TR2}$=21.2μmol/s, or $\dot{m}_{O2,TR2}$=677μg/s. Evidently, an insignificant fraction of the produced oxygen would reach even the shallowest of the three bed depths, to very slightly reoxidize the ceria. Put simply, if reduced oxide particles are covered by as little as 1cm of bed, they are mostly "protected" from reoxidation if their temperature decreases.

CONCLUSIONS

A detailed engineering design of pressure separation by packed columns of particles, in a solar thermochemical reactor prototype, shows that the concept is sound and robust under a multitude of varying conditions that may be encountered in operation, such as gas composition, void fraction, particle size distribution, and temperature. Some design limitations on bed heights and diameters, which exist in a small prototype, would not be present in a MW-sized device, thus likely enabling a simpler and even more robust design.

ACKGNOWLEDGEMENTS

This work is part of a project titled "High Efficiency Solar Thermochemical Reactor for Hydrogen Production", supported by the U.S. Department of Energy Fuel Cell Technologies Office. The authors gratefully acknowledge the contributions of our colleagues from Sandia National Laboratories, the German Aerospace Center, Bucknell University, and Arizona State University. Sandia is a multiprogram laboratory operated by Sandia Corporation, a Lockheed Martin Company, for the United States Department of Energy's National Nuclear Security Administration under Contract DE-AC04-94AL85000.

REFERENCES

1. T. Nakamura, Sol. Energy **19**, 467-475 (1977).
2. E. A. Fletcher and R. L. Moen, Science **197**, 1050-1056 (1977).
3. Y. Tamaura, A. Steinfeld, P. Kuhn, and K. Ehrensberger, Energy **20**, 325-330 (1995).
4. N. Gokon, S. Takahashi, H. Yamamoto, and T. Kodama, Int. J. Hydrogen Energy **33**, 2189-2199 (2008).
5. R. B. Diver, J. E. Miller, M. D. Allendorf, N. P. Siegel, and R. E. Hogan, J. Sol. Energy Eng. **130**, 041001-041001 -041001-041008 (2008).
6. J. Lapp, J. H. Davidson, and W. Lipinski, Energy **37**, 591-600 (2012).
7. I. Ermanoski, N. P. Siegel, and E. B. Stechel, J. Sol. Energy Eng. **135**, 031002-031001 - 031010 (2013).
8. I. Ermanoski, Int. J. Hydrogen Energy **39**, 13114-13117 (2014).
9. I. Ermanoski, et al., AIP Conference Proceedings **1734**, 120001 (2016).
10. I. Ermanoski, J. E. Miller, and M. D. Allendorf, PCCP **16**, 8418-8427 (2014).

11. I. Ermanoski, Energy Procedia **69**, 1731-1740 (2015).
12. L. I. Stiel and G. Thodos, Ind. Eng. Chem. Fundam. **2**, 233-& (1963).
13. J. V. Sengers and B. Kamgarparsi, J. Phys. Chem. Ref. Data **13**, 185-205 (1984).
14. E. Cunningham, Proc. R. soc. Lond. Ser. A-Contain. Pap. Math. Phys. Character **83**, 357-365 (1910).
15. Y. Ishida, Phys. Rev. **21**, 0550-0563 (1923).
16. M. Knudsen and S. Weber, Ann. Phys.-Berlin **36**, 983-996 (1911).
17. R. A. Millikan, Phys. Rev. **22**, 1-23 (1923).
18. R. A. Millikan, Phys. Rev. **21**, 217-238 (1923).
19. D. J. Rader, J. Aerosol. Sci. **21**, 161-168 (1990).
20.